Universiteit
Leiden
The Netherlands

Molecular and Nano-engineering with iron, ruthenium and carbon: Hybrid structures for sensing

Geest, E.P. van

Citation
Geest, E. P. van. (2021, January 14). *Molecular and Nano-engineering with iron, ruthenium and carbon: Hybrid structures for sensing*. Retrieved from https://hdl.handle.net/1887/139187

Version:	Publisher's Version
License:	Licence agreement concerning inclusion of doctoral thesis in the Institutional Repository of the University of Leiden
Downloaded from:	https://hdl.handle.net/1887/139187

Note: To cite this publication please use the final published version (if applicable).

Cover Page

Universiteit Leiden

The handle http://hdl.handle.net/1887/139187 holds various files of this Leiden University dissertation.

Author: Geest, E.P. van
Title: Molecular and Nano-engineering with iron, ruthenium and carbon: Hybrid structures for sensing
Issue Date: 2021-01-14

Chapter 7

[Ru(**3**)(biq)(STF-31)]$^{2+}$: A lock-and-kill anticancer PACT agent

*Ruthenium complexes have gained attention by the anticancer research community as potential prodrugs for photo-activated chemotherapy (PACT), but their fate in the cell is hard to trace because they are usually not emissive. We have developed a ruthenium prodrug that releases a fluorescent label, pyrene, when an ester linker installed between the ruthenium complex and the fluorophore is degraded by intracellular proteases. Upon hydrolysis of the ester linkage, the fluorescence of pyrene is no longer quenched by the complex, which allows for seeing the location of the prodrug and hence where irradiation with visible light should be realized. The complex, [Ru(**3**)(biq)(STF-31)](PF_6)$_2$, (where **3** = 3-([2,2′:6′,2″-terpyridin]-4′-yloxy)propyl-4-(pyren-1-yl)butanoate)) released the STF-31 ligand, a known cytotoxic nicotinamide phosphoribosyltransferase (NAMPT) inhibitor, upon light irradiation. The ester linker was found to be labile both under enzymatic and acidic conditions, which may allow for visualizing cancer cells specifically due to their higher drug metabolism and acidity. Confocal imaging and cell cytotoxicity should show if cells indeed become fluorescent upon treatment with the compound, and if the compound is more toxic after light irradiation. This new lock-and-kill principle could help to identify the malignant cells and hence know where to shine light for activating the compound, which will contribute to the development of photoactivated chemotherapy.*

E.P. van Geest, N. Salitra, S. Popal, R. Vadde, C. Van de Griend, G.F. Schneider and S. Bonnet, manuscript in preparation.

7.1. Introduction

Nowadays, a wide range of transition metals are considered for medicinal application against cancer, including platinum, palladium, copper, and ruthenium.[1] Many ruthenium drugs and prodrugs have been prepared, some of which have reached clinical trial.[2] In photodynamic therapy (PDT) and photoactivated chemotherapy (PACT), a ruthenium prodrug is activated upon visible light irradiation of the tumor, to induce cell death only at that place, while the complex when left in the dark is non-toxic, or much less toxic.[3] While PDT typically relies on the production of reactive oxygen species by energy or electron transfer to O_2 by the excited state of the ruthenium complex, in PACT the excited state releases a cytotoxic compound via a photosubstitution reaction independent of the presence of O_2. This specific mode of activation of PACT is relevant for oncology, as many tumors are hypoxic in their core, which makes them more difficult to treat.[4]

The cytotoxic species in PACT may be the ruthenium polypyridyl complex itself, but the complex may also be used as a photocage, to bind a toxic species which when bound is inactive, but can be activated by removing the ruthenium photocage.[5] A recent example from our group is the photoactivatable ruthenium complex [Ru(tpy)(biq)(STF-31)]$(PF_6)_2$, where tpy = 2,2′:6′2″-terpyridine, biq = 2,2′-biquinoline and STF-31 = 4-((4-*t*-butyl)phenylsulfonamido)methyl)-N-(pyridin-3-yl)benzamide.[6] This complex bears the biologically active STF-31 moiety, which is a known nicotinamide phosphoribosyltransferase (NAMPT) inhibitor.[7] When bound to the ruthenium metal center, STF-31 is 20 times less active than the free inhibitor. When the STF-31 molecule is released from the metal complex, it recovers its ability to inhibit NAMPT, which causes the cell to die.

Importantly, for efficient phototherapy in a patient, a surgeon needs to know where irradiation should be realized. PDT compounds (*i.e.*, protoporphyrin IX) are often luminescent, which is typically used to monitor the uptake of the PDT agent or to diagnose, using a strategy called photodynamic diagnosis (PDD),[8] but also to pinpoint where to shine light *in vivo*.[9] On the other hand, PACT compounds are generally not emissive.[10] Localizing where a PACT compound has been taken up is thus inherently difficult, which could potentially complicate the treatment of a cancer patient with PACT. To address this issue, we functionalized the [Ru(tpy)(biq)(STF-31)]$(PF_6)_2$ PACT complex with a fluorescent

tag by the attachment of a pyrene fluorophore to the tpy ligand *via* an intracellularly degradable ester linker. The complex [Ru(**3**)(biq)(STF-31)]$(PF_6)_2$ ([**1**]$(PF_6)_2$), where **3** = 3-([2,2′:6′,2″-terpyridin]-4′-yloxy)propyl-4-(pyren-1-yl)butanoate, is shown in Figure 7.1A. In this work, we present the synthesis and photochemical properties of [**1**]$(PF_6)_2$, and provide proof-of-concept that pyrene-based fluorescence can indeed be recovered through ester cleavage by esterases and under acidic conditions, thereby showing where the PACT complex should be irradiated. Ester cleavage in a living cell has been shown to occur quickly, which has been applied for prodrug activation, bio-imaging and uptake visualization,[11] and generally is faster in cancerous cells due to esterase overexpression.[12] Cancerous tissues are thus likely to light up more strongly than healthy tissue, giving an optical contrast which reveals the location of a tumor and shows where the irradiation should be done to kill the tumor through photo-activated release of STF-31 (Figure 7.1B-D).

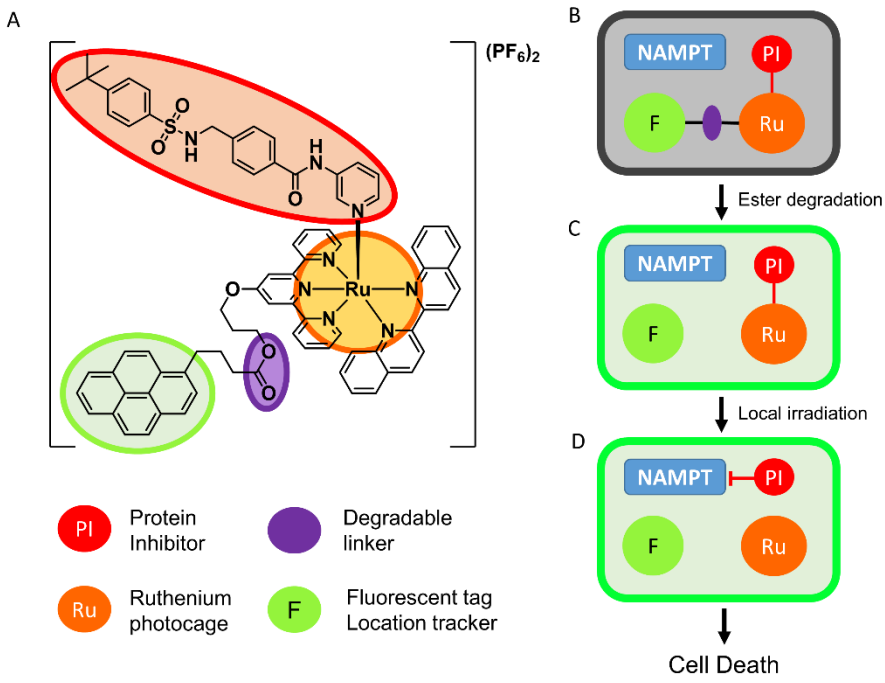

Figure 7.1: **A lock-and-kill PACT agent**. A) Molecular structure of [Ru(**3**)(biq)(STF-31)]$(PF_6)_2$ ([**1**]$(PF_6)_2$). The moieties with specific functionalities are highlighted in different colors. B-D) When the prodrug is internalized in a cell (B), the ester connection (violet) is cleaved by intracellular enzyme activity, which makes the fluorescence of the pyrene tag (green) no longer quenched by the ruthenium complex, hence lighting up the cell (C). The luminescent cells can then be treated by light irradiation, to release the STF-31 cytotoxic inhibitor (red) from the photocage (orange) and induce cell death (D).

7.2. Results and Discussion

7.2.1. Synthesis

[**1**](PF$_6$)$_2$ was synthesized using a modified protocol for making the fluorophore-free complex.[6] In short, 1,3-propanediol was reacted with 4′-chloro-2,2′:6′,2″-terpyridine to obtain compound **2** (see Scheme 7.1), to which pyrene was attached by esterification with 1-pyrenebutyric acid, to afford compound **3**. [(Ru(*p*-cymene)Cl$_2$)$_2$] was then reacted with ligand **3** to obtain [(Ru(**3**)Cl$_2$)$_2$] (compound [**4**]), which was converted into [Ru(**3**)(biq)Cl]Cl (compound [**5**]Cl) by coordination of 2,2′-biquinoline (biq). [**5**]Cl was then converted into [**1**](PF$_6$)$_2$ via substitution of the chlorido ligand for STF-31. As a reference, the same complex deprived of the pyrene moiety, [**8**](PF$_6$)$_2$, was prepared via the same route, but starting from ligand **2** instead of pyrene-functionalized ligand **3**. The reference complex [Ru(tpy)(biq)(STF-31)](PF$_6$)$_2$ ([**9**](PF$_6$)$_2$) was provided by R. Vadde.

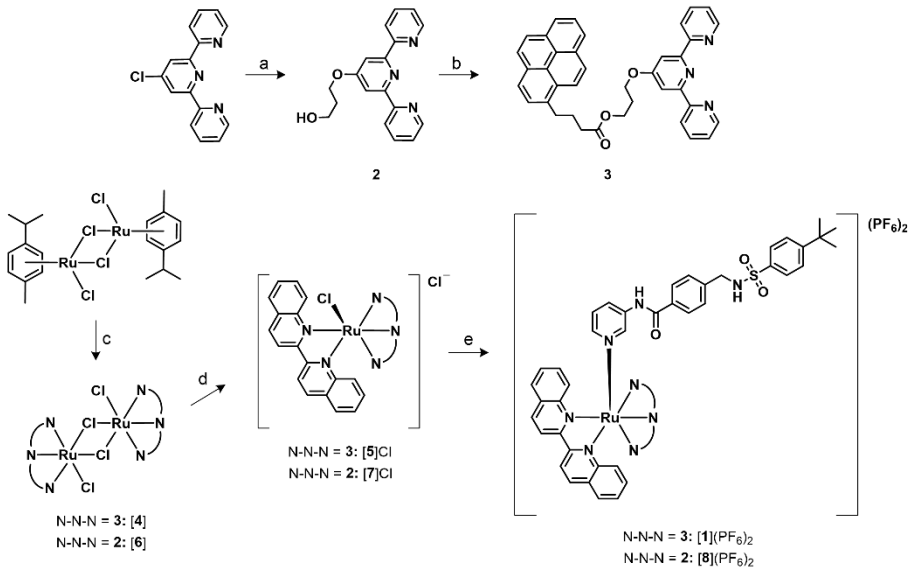

Scheme 7.1: Synthesis route towards [1](PF$_6$)$_2$ and [8](PF$_6$)$_2$. a) 1,3-propanediol, KOH, DMSO, 60 °C. b) 1-pyrenebutyric acid, DMAP, DCC, DCM, rt. c) compound **3** or **2**, DCM, rt. d) 2,2′-biquinoline, ethylene glycol, 180 °C. e) SFT-31, AgPF$_6$, acetone/water 1:1, 50 °C.

7.2.2. Photodriven release of STF-31

UV-vis spectroscopy was used to determine the photochemical properties of [**1**]$(PF_6)_2$. Although [**1**]$^{2+}$ is dicationic, the strongly hydrophobic ligands and PF_6 counter ions prevent complex [**1**]$(PF_6)_2$ from being soluble in water, so we used a methanol solution instead ([Ru] = 25 μM) to study photosubstitution of the STF-31 ligand by methanol upon irradiation. At first, the solution was kept in the dark while the absorbance was monitored over time; the absorbance profile did not change over 1 hour, showing the complex is stable in such conditions. After 1 hour, the solution was irradiated with green light (530 nm), upon which the absorbance spectra changed rapidly; within minutes λ_{max} shifted from 540 nm (pink solution) to 554 nm (purple solution) with a clear isosbestic point at 556 nm (see Figure S7.2A). Mass spectroscopy after irradiation confirmed that the starting complex was no longer present and the complex had been converted to the Ru-MeOH analogue (*m*/*z* = 483.6 and 966.4 for [**1** – STF-31 + MeOH]$^{2+}$ and [**1** – STF-31 + MeO]$^{+}$).

For complex [**8**]$(PF_6)_2$ we found very similar behavior to green light irradiation as observed for the pyrene-labelled compound [**1**]$(PF_6)_2$, as well as for the unmodified compound [**9**]$(PF_6)_2$ (Figure S7.1). The photosubstitution of STF-31 was rapid in all cases, as complete conversion was reached within 15 minutes of irradiation, *i.e.* the UV-vis spectra showed no change over time after 15 minutes (see Figure S7.2B) and MS showed that no starting material or only trace amounts remained after irradiation. The quantum yield (QY, the slope of the amount of the ruthenium STF-31 complex in solution *n* Ru-STF in mol over *Q*(t), the total amount of photons absorbed over time) for STF-31 photoexpulsion differs between the three complexes, however (see Figure S7.2C). For both ether-functionalized complexes [**1**]$(PF_6)_2$ and [**8**]$(PF_6)_2$ the quantum yield is very similar (QY = 0.0052 and 0.0058, respectively), while on the other hand, the unmodified complex [**9**]$(PF_6)_2$ has a higher quantum yield (QY = 0.012), similar to the value reported in water using red light (QY = 0.013).[6] On the one hand, the photosubstitution quantum yield is significantly influenced by ether functionalization of the tpy ligand. We think this effect is due to the electron-donating effect of the ether substituent on the terpyridine ligand, which likely increases the ligand field splitting energy, and hence the energy between the ^{3}MLCT and ^{3}MC state, thereby making ligand photosubstitution less likely to occur. On the other hand, however, the presence of the pyrene moiety on the

ether-modified tpy ligand of [**1**](PF$_6$)$_2$ has only little influence on the photoreactivity of the ruthenium complex.

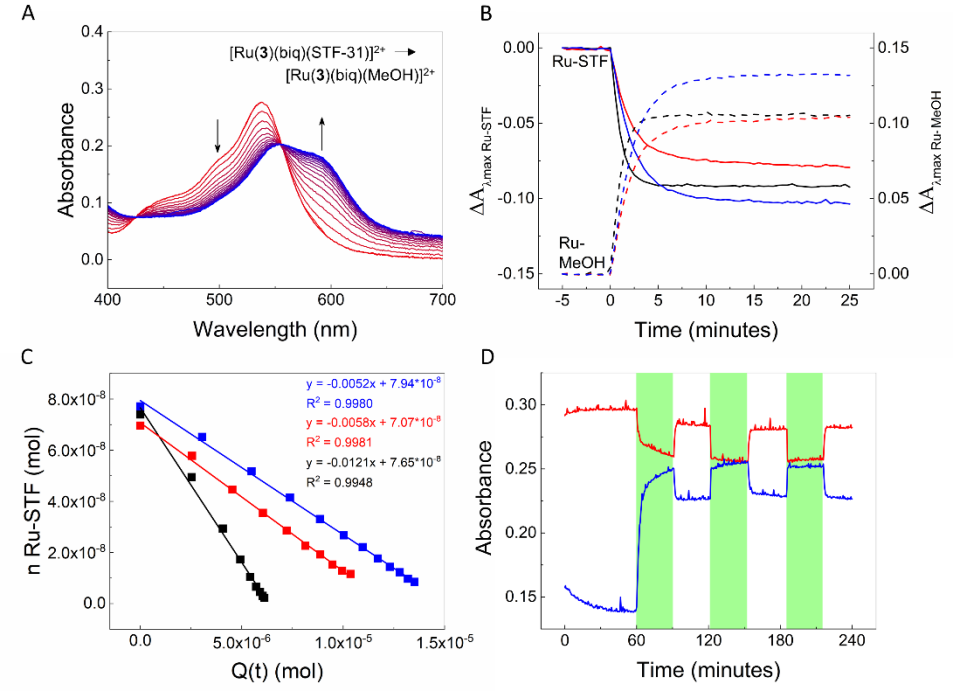

Figure 7.2: Photosubstitution of SFT-31. A) Evolution of absorbance of a solution of [**1**](PF$_6$)$_2$ in pure methanol (25 μM), upon irradiation with 530 nm light (photon flux = 1.36 x 10^{-7} mol·s^{-1}) after 1 h equilibration in the dark. Spectra show the absorbance at the start of irradiation (red) to 10 minutes after irradiation started (blue), recorded every 30 seconds. B) Absorbance change ΔA over time at λ_{max} for [**1**](PF$_6$)$_2$, [**8**](PF$_6$)$_2$, and [**9**](PF$_6$)$_2$ in the dark (denominated Ru-STF: blue, red and black solid line, resp. 540, 538 and 531 nm), and for their corresponding photoproducts (denominated Ru-MeOH: blue, red and black dashed line, resp. 554, 552 and 580 nm). C) Evolution of the amount of Ru-STF complexes in solution, *n* Ru-STF in mol, *vs.* the total amount of photons absorbed by the Ru-STF complexes since t = 0, *Q*(t) in mol, for [**1**](PF$_6$)$_2$, [**8**](PF$_6$)$_2$, and [**9**](PF$_6$)$_2$ (blue, red and black); the slope of these plots are the quantum yields of the photosubstitution in pure methanol. D) Absorbance *vs.* time at absorption maximum λ_{max} for [**1**](PF$_6$)$_2$ and the photoproduct (red and blue, λ_{max} = 540 and 587 nm, respectively) in a 95:5 methanol/water mixture. Irradiation started at t = 60 min and was switched off and on (green bars) repeatedly, every 30 min. Spectra were recorded every 30 seconds.

For all three complexes, STF-31 photosubstitution in methanol is an irreversible process, *i.e.* when light was switched off, no back-coordination of STF-31 to the ruthenium methanol complex was observed. However, when the same experiment was carried out in presence of 5% water (MeOH/H$_2$O 95:5), the photoreaction became reversible, as demonstrated by UV-vis spectroscopy upon alternatively switching on and off a source of light and monitoring the spectrum

of the solution (see Figure S7.2D and Figure S7.2). The obtained reversibility by adding water could be due to solvation effects: in pure methanol, the liberated STF-31 and the ruthenium photoproduct are very soluble and can thus diffuse away from each other, which inhibits them from reacting again to form [**1**]$^{2+}$. However with water present the reaction products, which are sparsely soluble in water, diffuse less than in methanol, as they are kept close to each other in a solvent 'cage' by the water molecules, and the back-reaction is thus more likely to occur.[13] Such reversibility, though interesting, is probably not a problem in a biological setting: cells are full of hydrophobic regions (proteins, membranes, DNA, etc.), which would be capable of solvating the photoproducts of photosubstitution in [**1**]$^{2+}$. Overall, all three complexes release the STF-31 ligand upon green light irradiation, and adding the pyrene group did not prevent this photosubstitution to occur.

7.2.3. Unlocking fluorescence by releasing pyrene

As pyrene and the ruthenium complex can be studied independently by shining UV or visible light, respectively, it was also possible to study the effect of the ruthenium complex on pyrene emission. Initially, we hypothesized that the presence of the ester linker would be detrimental for the emission properties of the pyrene group, and that such quenching by the ruthenium complex would be relieved when the ester linker is cleaved (see Figure 7.3A). In order to test this hypothesis, we first studied the luminescence properties of the intact complex [**1**]$(PF_6)_2$ and [**5**]Cl (the complexes with and without STF-31), and that of the ester degradation products [**7**]Cl and 1-pyrenebutyric acid in methanol. [**1**]$(PF_6)_2$ was found to be not fluorescent, while complex [**5**]Cl showed weak emission at 395 nm and 375 nm upon excitation at 354 nm. On the other hand, upon mixing 1-pyrenebutyric acid and [**7**]Cl at the same concentration (50 μM), strong emission was observed at 395 and 375 nm, showing that pyrene quenching by an unbound ruthenium complex is not very strong (see Figure 7.3B and Figure S7.3). It did occur to some extent though, as 1-pyrenebutyric acid alone showed stronger fluorescence at 375 to 400 nm in absence of any ruthenium complex. As the ruthenium complex absorbs in the region where free pyrene emits (see Figure 7.3C), and fluorescence quenching was much stronger when pyrene is covalently attached to the complex, quenching likely occurs *via* Förster resonance energy transfer (FRET), similar to the quenching mechanism for a similar pyrene-labeled ruthenium(II) trisbipyridine complex.[14] We calculated the Förster distance R_0 (see

appendix Chapter 7), at which quenching of the fluorescence by FRET is 50%, for the donor/acceptor pair 1-pyrenebutyric acid/[**8**](PF$_6$)$_2$ in methanol, and found R_0 = 24.4 Å, while in a model of [**1**]$^{2+}$ (simulated with Yasara, see Figure S7.4) we found the Ru-pyrene distance to be 20 Å, which confirms that pyrene is quenched by FRET in our system. Moreover, we calculated the FRET efficiency φ_{FRET} for 1-pyrenebutyric acid/[**8**](PF$_6$)$_2$ and found that φ_{FRET} = 0.77, hence FRET quenching is efficient. Overall, in methanol the fluorescence of pyrene is indeed quenched by its ruthenium neighbor when pyrene is covalently attached to the ruthenium complex, and quenching occurs through the FRET mechanism.

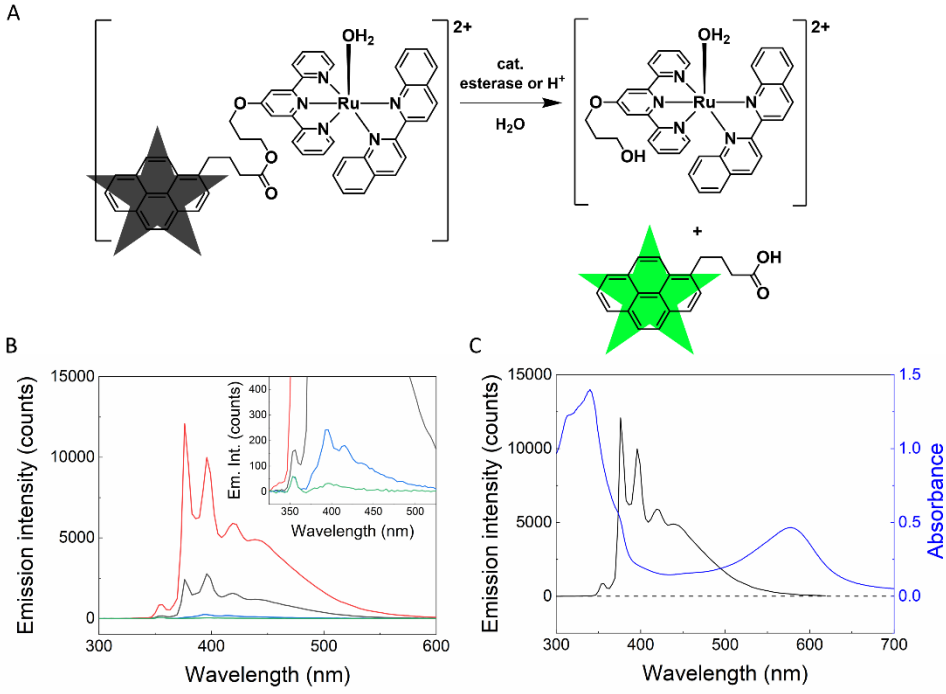

Figure 7.3: Quenching of pyrene emission by ruthenium. A) Upon cleavage of the ester bond, the initially quenched pyrene (black star) is liberated as free 1-pyrenebutyric acid, which is no longer quenched by the ruthenium complex and shows strong fluorescence (green star). B) Emission intensity of a methanol solution of [**1**](PF$_6$)$_2$ (green), of [**5**]Cl (blue), of a 1:1 mixture of [**7**]Cl and 1-pyrenebutyric acid (black), and of 1-pyrenebutyric acid alone (red), all excited at 354 nm. Concentration of all species was 50 μM. Inset: zoom of emission intensity (Em. Int.). C) Spectral overlap between the emission of 1-pyrenebutyric acid (black, left axis, excited at 354 nm) and absorbance of [**7**[Cl (blue, right axis), both 50 μM in methanol. Dashed line is the baseline.

7.2.4. Ester degradation

To study if the ester connection between the ruthenium complex and pyrene can indeed be degraded in aqueous solutions by esterase activity to release free pyrene and obtain fluorescence, we carried out a relatively simple experiment with [**5**]Cl, as [**1**]$(PF_6)_2$ is insoluble in water: to a solution of [**5**]Cl (1 mM in water) fresh, filtered human saliva was added, which is known to have esterase activity, among other enzyme activities.[15] The solution was stirred at 37 °C and the luminescence was measured at different time points (3, 24, 48, 72, 120 and 168 hours, final [Ru] = 50 μM; Ru/saliva solution volume ratio = 1:19). As a purple precipitation occurred, the sample was centrifuged at 4000 rpm for 10 minutes and the luminescence of the supernatant was measured. An increase of emission in the emission range of 375-450 nm, resembling the emission of pyrene (excited at 354 nm) within 24 hours indicated that the ester connection was hydrolysed and pyrene was liberated (see Figure 7.4A and Figure S7.5), unlike a solution [**5**]Cl without the enzymes or the solution of saliva alone itself. Thus, the ester bond of [**5**]Cl is indeed degraded by enzyme activity, which recovers the emission properties of the liberated pyrene moiety.

The acid sensitivity of the ester linker in [**5**]Cl was also demonstrated in a separate crystallization experiment. When a solution of [**5**]Cl in methanol was acidified with triflic acid, single crystals were obtained that were suitable for X-ray structure determination. The obtained crystal structure showed the formed crystals to be of the complex [Ru(**2**)(biq)(OH_2)]$(OTf)_2$ (see Figure 7.4B). The large torsion angle over N3-Ru1-N1-C1 (107.1°) shows that the biq ligand is tilted with respect to ligand **2**, likely due to steric effects,[16] as the Ru1-N1 bond (2.102 Å) from biq is relatively long compared to the Ru1-N4 (1.990 Å) bond (see Table 7.1). Most importantly, the crystal structure revealed that the ester bond between pyrene and ruthenium in [**5**]Cl is also cleaved in acidic conditions. Overall, [**1**]$(PF_6)_2$ can hence release two fragments: a NAMPT inhibitor, when the complex is irradiated with visible light; and a pyrene group, when the ester bond in the complex is cleaved either by esterases or acid, upon which the pyrene group becomes fluorescent as it is no longer quenched by the covalently attached ruthenium complex.

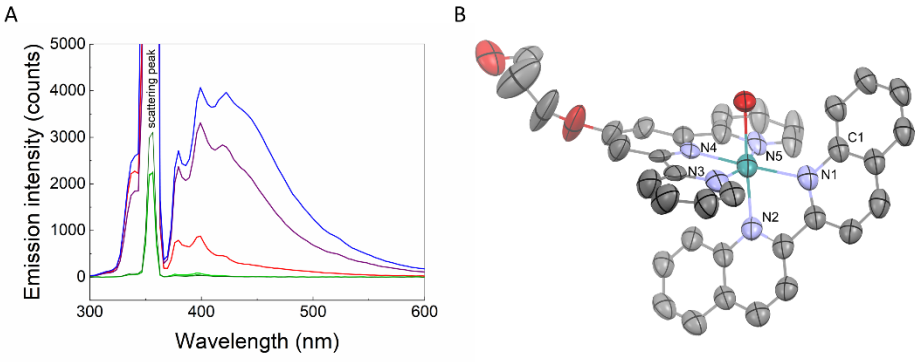

Figure 7.4: Fluorescence activation. A) Luminescence intensity *vs.* emission wavelength, excited at 354 nm, for a mixture of **[5]**Cl (50 μM) and saliva at 3 h, 24 h and 48 h (red to blue) and the same complex in water at the same concentration and time points (dark to light green). The peak at 354 nm is due to light scattering. B) Displacement ellipsoid plot (50% probability) of the structure of [Ru(**2**)(biq)(OH_2)](OTf)$_2$, obtained from a solution of **[5]**Cl in a methanol that was acidified with triflic acid. Hydrogen atoms and the triflate counter ions have been omitted for clarity.

Table 7.1: Selected bond lengths (Å) and torsion angle (°) for [Ru(2)(biq)(OH_2)](OTf)$_2$.

[Ru(**2**)(biq)(OH_2)](OTf)$_2$			
Ru1-N1	2.102(6)	Ru1-N4	1.990(8)
Ru1-N2	2.073(5)	Ru1-N5	2.087(8)
Ru1-N3	2.080(2)	N3-Ru1-N1-C1	107.1(6)

7.3. Conclusions & Outlook

Ruthenium complex **[1]**(PF_6)$_2$ was synthesized, bearing a hydrolysable pyrene fluorophore and a light-cleavable STF-31 ligand. Upon green light irradiation in methanol, STF-31 is photosubstituted by a solvent molecule. The presence of the pyrene group does not affect the kinetics of this photoreaction, but the presence of the ruthenium complex strongly quenches the fluorescence of the pyrene moiety. When the ester linker between the ruthenium complex and the pyrene moiety is cleaved, catalyzed either by esterases or acid, the fluorescence of the pyrene tag is "unlocked". We envision that this principle could be used for visualizing prodrug uptake in cancer cells, which are more acidic and contain highly active esterases. Light activation of the PACT prodrug should be realized by specifically aiming the laser at fluorescent cells, which, if this concept can be translated *in vivo*, may allow for having a highly selective anticancer action.

To further demonstrate that this principle will work in a biological context, confocal studies should be first done *in vitro* to see if cells indeed light up after drug uptake, while confocal microscopy with full living organisms, *i.e.* zebrafish embryo or mice, may show whether the cancer tissues light up more strongly due to prodrug uptake, compared to non-cancerous tissues. Finally, cytotoxicity studies should be done with [**1**]$(PF_6)_2$, possibly in a liposomal formulation to increase the water solubility of the complex and ease administration, to assess the difference in anticancer efficacy of the drug between dark and light irradiation conditions.

7.4. References and Notes

[1] K. D. Mjos, C. Orvig, *Chem. Rev.* **2014**, *114*, 4540.

[2] M. J. Clarke, *Coord. Chem. Rev.* **2002**, *232*, 69; R. E. Morris, R. E. Aird, P. D. Murdoch, H. M. Chen, J. Cummings, N. D. Hughes, S. Parsons, A. Parkin, G. Boyd, D. I. Jodrell, P. J. Sadler, *J. Med. Chem.* **2001**, *44*, 3616; G. Sava, S. Zorzet, C. Turrin, F. Vita, M. Soranzo, G. Zabucchi, M. Cocchietto, A. Bergamo, S. DiGiovine, G. Pezzoni, L. Sartor, S. Garbisa, *Clin. Cancer Res.* **2003**, *9*, 1898; S. Monro, K. L. Colón, H. Yin, J. Roque, P. Konda, S. Gujar, R. P. Thummel, L. Lilge, C. G. Cameron, S. A. McFarland, *Chem. Rev.* **2019**, *119*, 797.

[3] C. Mari, V. Pierroz, S. Ferrari, G. Gasser, *Chem. Sci.* **2015**, *6*, 2660; R. Friederike, S. Wiktor, *Curr. Med. Chem.* **2017**, *24*, 4905; C. Mari, V. Pierroz, R. Rubbiani, M. Patra, J. Hess, B. Spingler, L. Oehninger, J. Schur, I. Ott, L. Salassa, S. Ferrari, G. Gasser, *Chem. Eur. J.* **2014**, *20*, 14421.

[4] S. Bonnet, *Dalton Trans.* **2018**, *47*, 10330; P. Vaupel, A. Mayer, *Cancer Metastasis Rev.* **2007**, *26*, 225.

[5] J.-A. Cuello-Garibo, M. S. Meijer, S. Bonnet, *Chem. Commun.* **2017**, *53*, 6768; A. Li, R. Yadav, J. K. White, M. K. Herroon, B. P. Callahan, I. Podgorski, C. Turro, E. E. Scott, J. J. Kodanko, *Chem. Commun.* **2017**, *53*, 3673; B. A. Albani, B. Peña, N. A. Leed, N. A. B. G. de Paula, C. Pavani, M. S. Baptista, K. R. Dunbar, C. Turro, *J. Am. Chem. Soc.* **2014**, *136*, 17095; R. N. Garner, J. C. Gallucci, K. R. Dunbar, C. Turro, *Inorg. Chem.* **2011**, *50*, 9213.

[6] L. N. Lameijer, D. Ernst, S. L. Hopkins, M. S. Meijer, S. H. C. Askes, S. E. Le Dévédec, S. Bonnet, *Angew. Chem., Int. Ed.* **2017**, *56*, 11549.

[7] D. Kraus, J. Reckenbeil, N. Veit, S. Kuerpig, M. Meisenheimer, I. Beier, H. Stark, J. Winter, R. Probstmeier, *Cell. Oncol.* **2018**, *41*, 485.

[8] I. Kausch, M. Sommerauer, F. Montorsi, A. Stenzl, D. Jacqmin, P. Jichlinski, D. Jocham, A. Ziegler, R. Vonthein, *Eur. Urol.* **2010**, *57*, 595; Y. Matoba, K. Banno, I. Kisu, D. Aoki, *Photodiagn. Photodyn. Ther.* **2018**, *24*, 52; H. Fukuhara, S. Yamamoto, T. Karashima, K. Inoue, *Int. J. Clin. Oncol.* **2020**; Z. Malik, *Transl. Biophotonics* **2020**, *2*, e201900022; H. Kostron, *Photodynamic Diagnosis and Therapy for Brain Malignancies from the Bench to Clinical Application,* in *Photodynamic Therapy: From Theory to Application*, Springer Berlin Heidelberg, **2014**, 165.

[9] S. Mallidi, B. Q. Spring, S. Chang, B. Vakoc, T. Hasan, *Cancer J.* **2015**, *21*, 194.

[10] B. Siewert, M. Langerman, Y. Hontani, J. T. M. Kennis, V. H. S. van Rixel, B. Limburg, M. A. Siegler, V. Talens Saez, R. E. Kieltyka, S. Bonnet, *Chem. Commun.* **2017**, *53*, 11126.

[11] B. Rotman, B. W. Papermaster, *Proc. Natl. Acad. Sci. U. S. A.* **1966**, *55*, 134; L. D. Lavis, T.-Y. Chao, R. T. Raines, *ACS Chem. Biol.* **2006**, *1*, 252; C. Molenaar, J.-M. Teuben, R. J. Heetebrij, H. J. Tanke, J. Reedijk, *JBIC, J. Biol. Inorg. Chem.* **2000**, *5*, 655; B. M. Liederer, R. T. Borchardt, *J. Pharm. Sci.* **2006**, *95*, 1177.

[12] H. Dong, L. Pang, H. Cong, Y. Shen, B. Yu, *Drug Delivery* **2019**, *26*, 416; E. Afrimzon, A. Deutsch, Y. Shafran, N. Zurgil, J. Sandbank, I. Pappo, M. Deutsch, *Clin. Exp. Mestastas.* **2008**, *25*, 213.
[13] R. Breslow, *Acc. Chem. Res.* **1991**, *24*, 159.
[14] M. Vonlanthen, A. Cevallos-Vallejo, E. Aguilar-Ortíz, A. Ruiu, P. Porcu, E. Rivera, *Polymer* **2016**, *99*, 13.
[15] H. Yamahara, V. H. L. Lee, *Adv. Drug Delivery Rev.* **1993**, *12*, 25.
[16] D. M. Klassen, *Inorg. Chem.* **1976**, *15*, 3166.